Supplementary Information

Energy-Distinguishable Bipolar UV Photoelectron Injection from LiCl-Promoted $FAPbCl_3$ Perovskite Nanorods

Jue Gong[a], Xun Li[a], Peijun Guo[b], Ian Zhang[a], Wei Huang[c,d], Ke Lu[a], Yingwen Cheng[a], Richard D. Schaller[b,c], Tobin J. Marks[c,d], Tao Xu[a,*]

[a]Department of Chemistry and Biochemistry, Northern Illinois University, DeKalb, IL 60115 United States

[b]Center for Nanoscale Materials, Argonne National Laboratory, Argonne, IL 60439, United States

[c]Department of Chemistry, [d]Materials Research Center, Northwestern University, 2145 Sheridan Road, Evanston, IL 60208, United States

* Corresponding author

Prof. Tao Xu (Email: txu@niu.edu)

Keywords: perovskite, nanostructure, photodetector, X-ray photoelectron spectroscopy, ultraviolet photoelectron spectroscopy

Methods

Chemicals and precursor

Hydrochloric acid (HCl, 37.0%) and ethyl ether (anhydrous) were purchased from Fisher Chemical. Lead(II) chloride ($PbCl_2$, 99.999%), formamidine acetate salt ($HC(NH_2)NH{\cdot}HCOOCH_3$, 99%), 2-propanol (anhydrous, 99.5%) and dimethyl sulfoxide (DMSO, anhydrous, 99.9+%) were purchased from Aldrich. All chemicals were used as received without purification. $HC(NH_2)_2Cl$ (FACl) was synthesized by reacting 1.1:1 molar ratio of HCl and

$HC(NH_2)NH{\cdot}HCOOCH_3$ in a 100-mL round bottom flask immersed in ice bath, as followed by rotary evaporation at 60 ˚C to dry off the solvent. As-formed solid was then washed with copious amount of ethyl ether and accompanied with vacuum filtration. Finally, pure FACl product was obtained by drying in a vacuum oven at 60 ˚C overnight.

Synthesis of $FAPbCl_3$ and LiCl:$FAPbCl_3$ nanorods

The growth of $FAPbCl_3$ and LiCl:$FAPbCl_3$ nanostructures followed the methods reported in literatures[1,2] with adaptations. In detail, 100 mg/mL $PbCl_2$/DMSO solution was first spun-coated on acetone-cleaned FTO glass (Pilkington Glass) at 1000 rpm for 10 seconds. The as-formed wet film was then quickly transferred to a 50-mL ethyl ether bath for 5 minutes. Crystallized $PbCl_2$ film was then annealed on a hot plate at 100 ˚C for about 30 minutes, before being dipped into 10 mg/mL FACl or 10 mg/mL FACl & 1 mg/mL LiCl in 2-propanol solutions (with lead precursor coated sides facing down) for respectively synthesizing pristine $FAPbCl_3$ or LiCl:$FAPbCl_3$ nanorods for 24 hours.

Perovskite UV photodetectors

Gold layers were deposited on the as-prepared perovskite/FTO substrates with a thermal evaporator (Edward 306 A) to finish construction of the UV photodetectors. 365-nm UVL-4F UV lamp was utilized to generate photocurrents without magnitude oscillation, while UVGL-25 Multiband UV lamp with 254/365 nm wavelengths was used to generate photocurrents with damping magnitudes. Photocurrents were collected under chronoamperometry on a CH Instrument potentiostat under sample period of 0.001 s or 0.01 s, with equilibration time of 5 s and zero voltage bias. Potentiostatic electrochemical impedance spectroscopy was performed on a Gamry Reference 600 potentiostat to measure Nyquist plots of LiCl:$FAPbCl_3$ photodetector, under

parameters of 10-s initial delay, 100000-Hz initial frequency, 0.001-Hz final frequency, 10 points/decade, AC voltage of 5 mV·rms and zero DC voltage vs. open-circuit voltage.

Structural, morphological and optical characterizations

X-ray diffracion patterns of perovskite nanostructured films were collected from 10-50˚ of 2θ using a Bruker D2 Phaser Diffractometer with a sampling speed of 0.1˚/s. Microscopic images of synthesized perovskite nanorods were taken with a scanning electron microscope (TESCAN, Vega II SBH) under 5.21-kx magnification. Optical reflectance was performed with a Filmetrics F20-EXR thin-film analyzer, with spectral range of 380 to 1700 nm. Fluorescence was measured with a Hitachi F-2500 fluorescence spectrophotometer equipped with xenon lamp as light source, where a 350-nm excitation (2.5-nm slit width) was applied to collect emissions (2.5-nm slit width) of perovskite nanostructured films with a scan speed of 15 nm/minute from 350 to 550 nm spectral range.

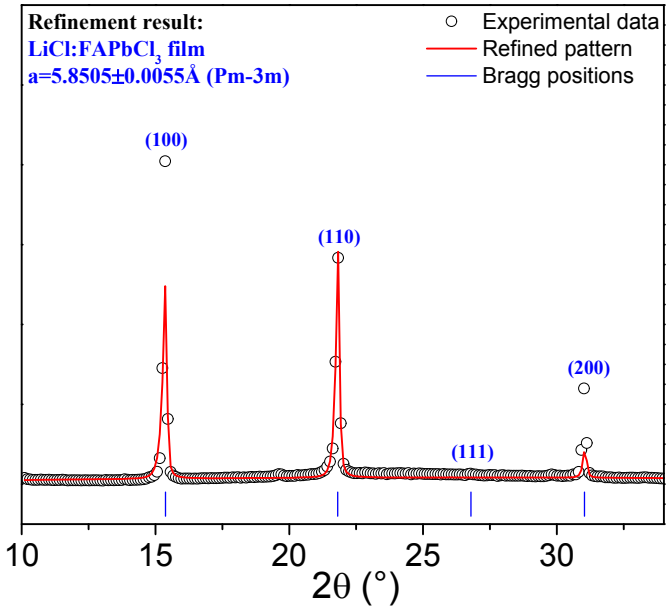

Fig. S1 XRD refinement of LiCl:$FAPbCl_3$ nanostructured film against reported cubic $FAPbCl_3$ (Pm-3m)[3], with a refined cell parameter being 5.8505±0.0055 Å.

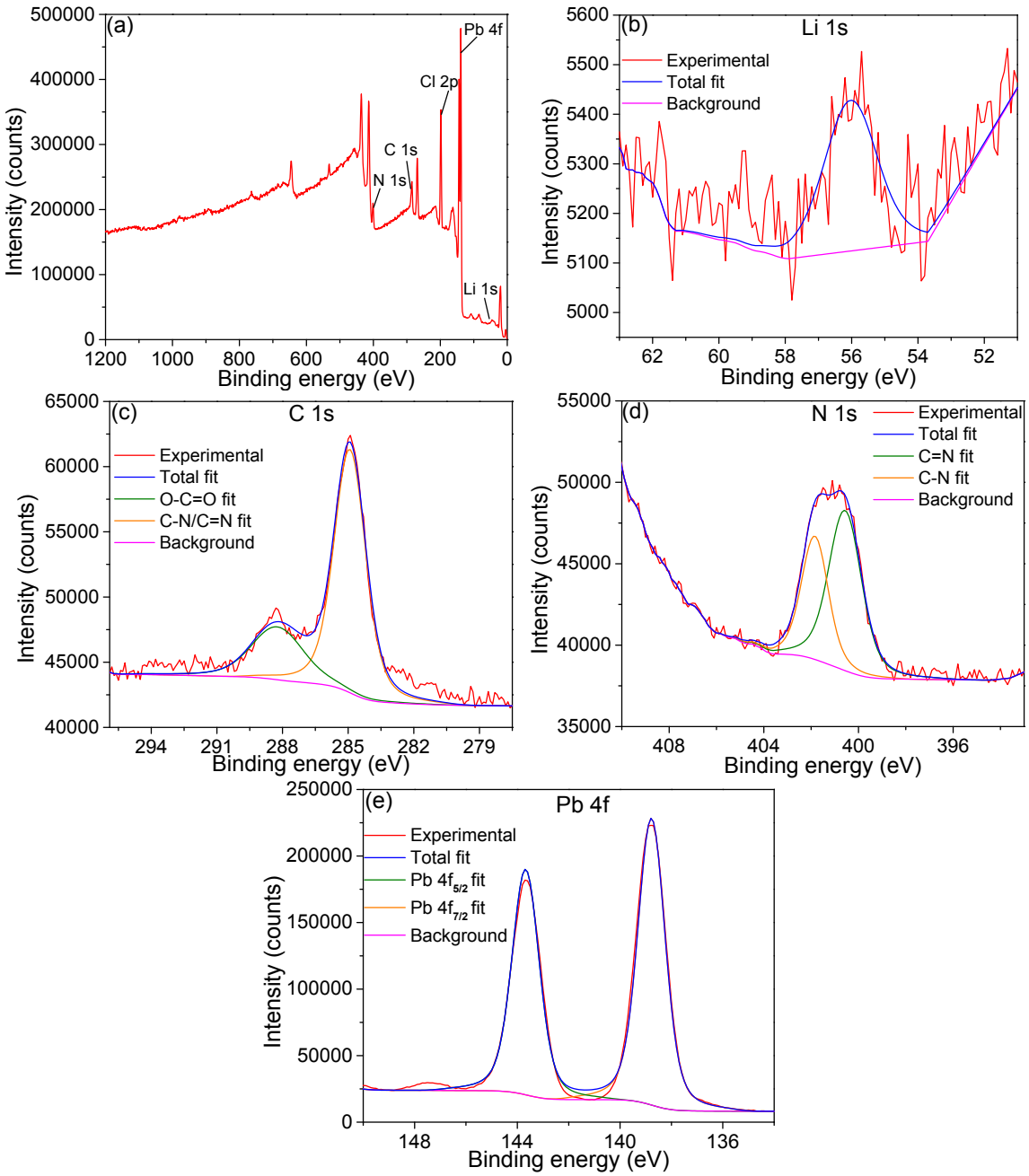

Fig. S2 X-ray photoelectron spectra of LiCl:$FAPbCl_3$ nanostructured film. (a) Survey scan of LiCl:$FAPbCl_3$ sample. Resolution scans of (b) Li 1s, (c) C 1s, (d) N 1s and (e) Pb 4f electrons.

Table S1. Calculated atomic compositions of scanned elements from XPS measurements of LiCl:$FAPbCl_3$ nanostructured film.

Name	Binding energy (eV)	FWHM (eV)	Area (CPS·eV)	Atomic (%)
C1s Scan A	283.90	1.78	35905.47	0.00
C1s Scan B	287.16	2.81	14039.63	0.00
C1s Combined	0.00	0.00	49945.10	53.70
Li1s Scan A	55.03	1.85	609.94	9.97
Pb4f 7/2 Scan A	137.78	1.36	307474.25	16.41
Pb4f 5/2 Scan A	142.68	1.36	241776.69	0.00
N1s Scan A	400.86	1.45	11945.82	0.00
N1s Scan B	399.54	1.69	17740.83	0.00
N1s Combined	0.00	0.00	29686.65	19.92

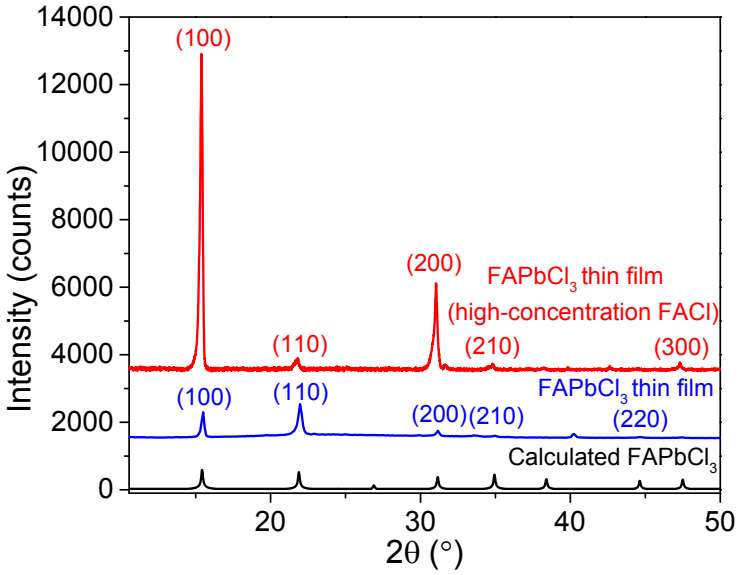

Fig. S3 Comparison of XRD pattern of high-concentration FACl-promoted $FAPbCl_3$ (red) with low-concentration FACl-promoted counterpart (blue, Fig. 1a), and calculated $FAPbCl_3$ reference[3] (black).

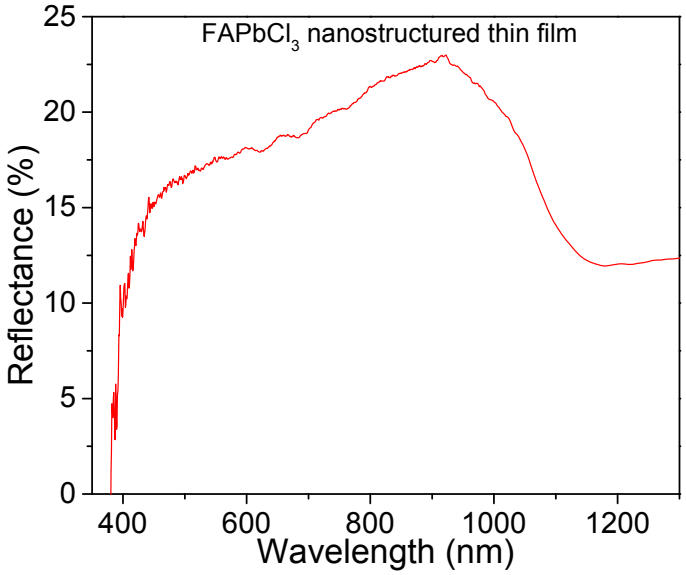

Fig. S4 Optical reflectance spectrum of $FAPbCl_3$ nanostructured thin film.

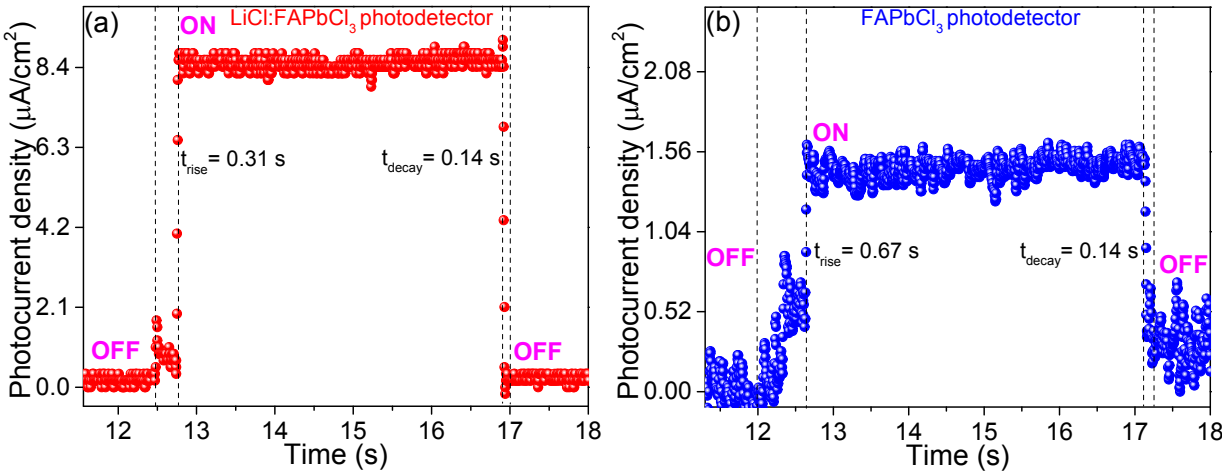

Fig. S5 Rise and decay kinetics of photocurrents on LiCl:$FAPbCl_3$ (a) and $FAPbCl_3$ (b) UV photodetectors.

Table S2. Summary of materials applied in UV photodetectors with corresponding performance parameters.

Material	Wavelength (nm)	Responsitivity	Rise time	Decay time	Reference
ZnO thin film	380	0.1 mA/W	48 s	0.9 s	4, 5
ZnO nanocrystal	370	61 A/W	0.1 s	1 s	6, 7
ZnO-SnO_2 nanofibers	300	/	32.2 s	7.8 s	6, 8
GaN film	325	340 mA/W	0.28 s	0.45 s	6, 9
NiO film	365	4.5 A/W	0.266 s	0.2 s	6, 10
TiO_2 thin film	260	199 A/W	6 s	15 s	4, 11
$SrTiO_3$ single crystal	330	213 mA/W	1.3 ns	/	4, 12
$LaAlO_3$ single crystal	200	71.8 mA/W	/	/	4, 13
$LiNbO_3$ single crystal	300	17.1 mA/W	0.5 ns	/	4, 14
$LiTaO_3$ single crystal	235	2 mA/W	0.2 ns	/	4, 15
ZnO/$SrTiO_3$ heterostructure	365	/	/	/	4, 16
$TbMnO_3$/Nb-$SrTiO_3$ heterostructure	365	/	510 ns	/	4, 17
$MAPbCl_3$ single crystal	365	46.9 mA/W	24 ms	62 ms	4
$MAPbCl_3$ single crystal	255	450 mA/W	15 ms	55 ms	18
$MAPbBr_3$ single crystal	255	300 mA/W	2.5 ms	2.5 ms	18
$MAPbI_3$ single crystal	255	120 mA/W	2 ms	2 ms	18
$MAPbCl_3$ thin film	360	7.56 A/W	170 μs	220 μs	19
$CsPbCl_3$ nanocrystal thin film	365	1.89 A/W	41 ms	43 ms	6
$FAPbCl_3$ nanorod film	365	29 mA/W	0.67 s	0.14 s	This work
LiCl:$FAPbCl_3$ nanorod film	365	167 mA/W	0.31 s	0.14 s	This work

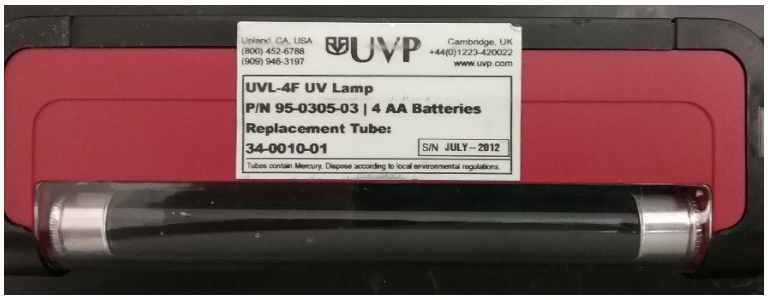

Fig. S6 Picture of the DC-powered UV lamp, which operates on constant current from 4 AA batteries.

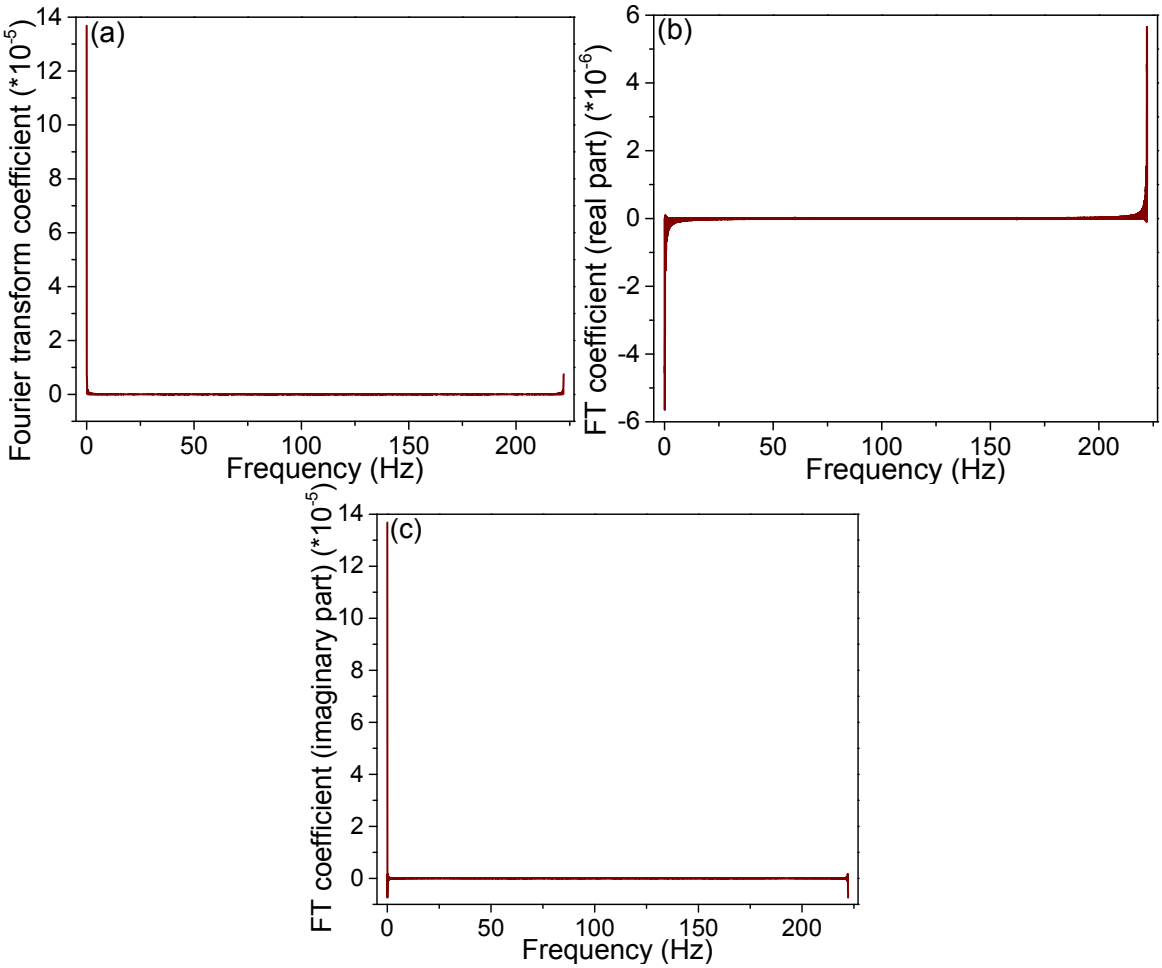

Fig. S7 Fourier transform of transient photocurrents of LiCl:$FAPbCl_3$ nanorod film shown in Figure 2a. (a) Fourier transform coefficient plot. (b) Real-part Fourier transform coefficient plot. (c) Imaginary-part Fourier transform coefficient plot.

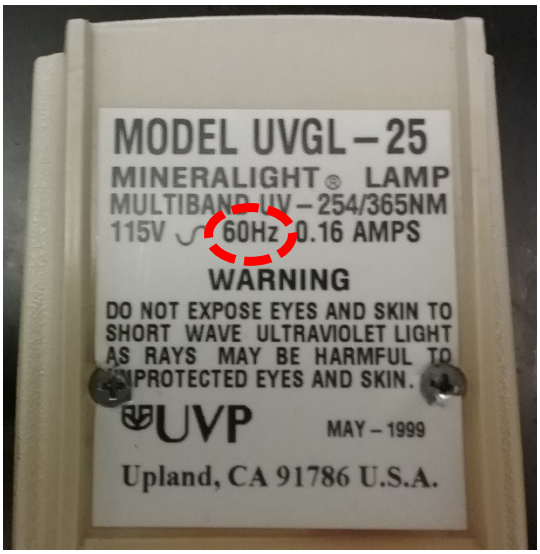

Fig. S8 Picture of the AC-powered UV lamp, which operates on 60-Hz oscillating current.

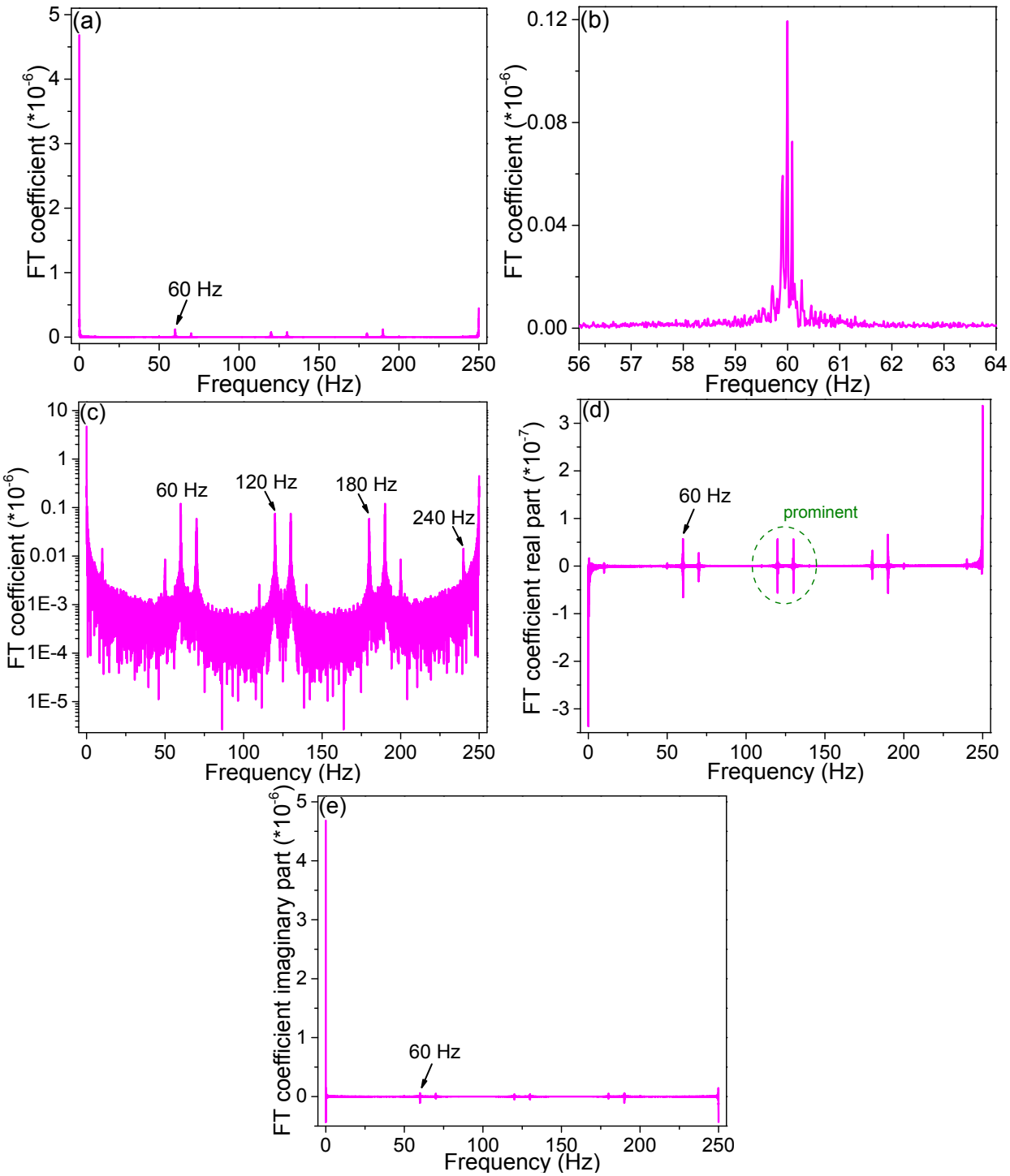

Fig. S9 Fourier transform of on-off photocurrents of LiCl:$FAPbCl_3$ nanostructured film achieved under 365-nm AC-powered UV illumination. (a) Fourier transform coefficient plot. (b) Zoomed-in view of the coefficient plot in the range of 56 to 64 Hz. (c) Logarithmic scale of coefficient plot. (d) and (e) Real-part and imaginary-part coefficient plots, respectively.

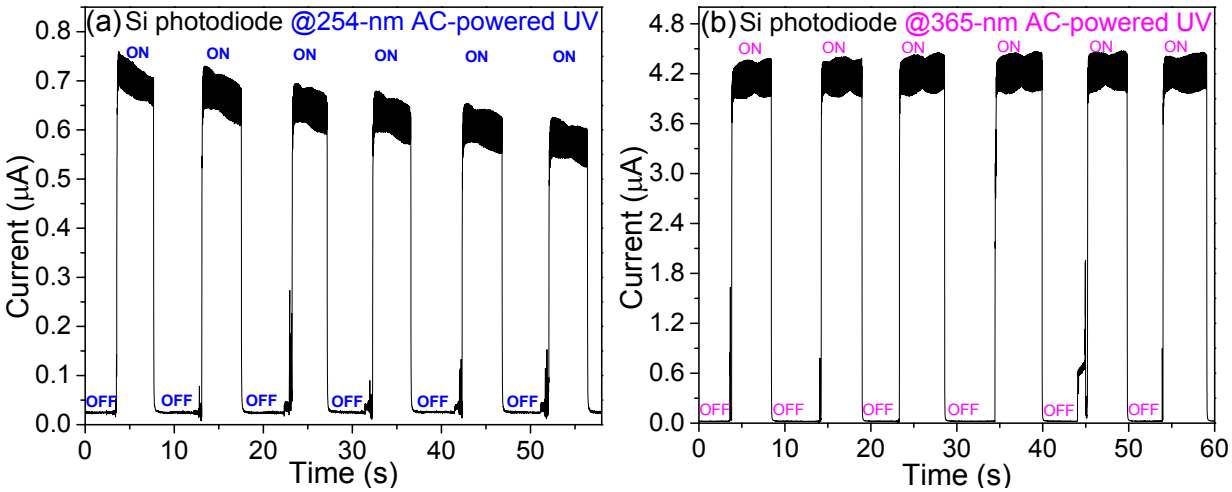

Fig. S10 On-off photocurrents of Si photodiode under 254-nm (a) and 365-nm (b) AC-powered UV illuminations with sampling period of 0.01 s.

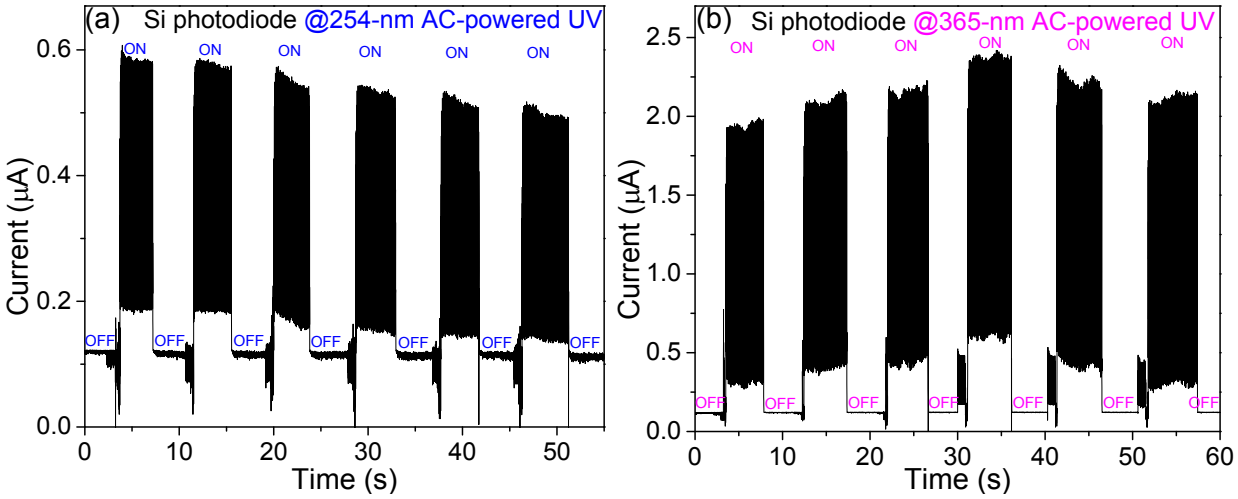

Fig. S11 On-off photocurrents of Si photodiode under 254-nm (a) and 365-nm (b) AC-powered UV illuminations with sampling period of 0.001 s.

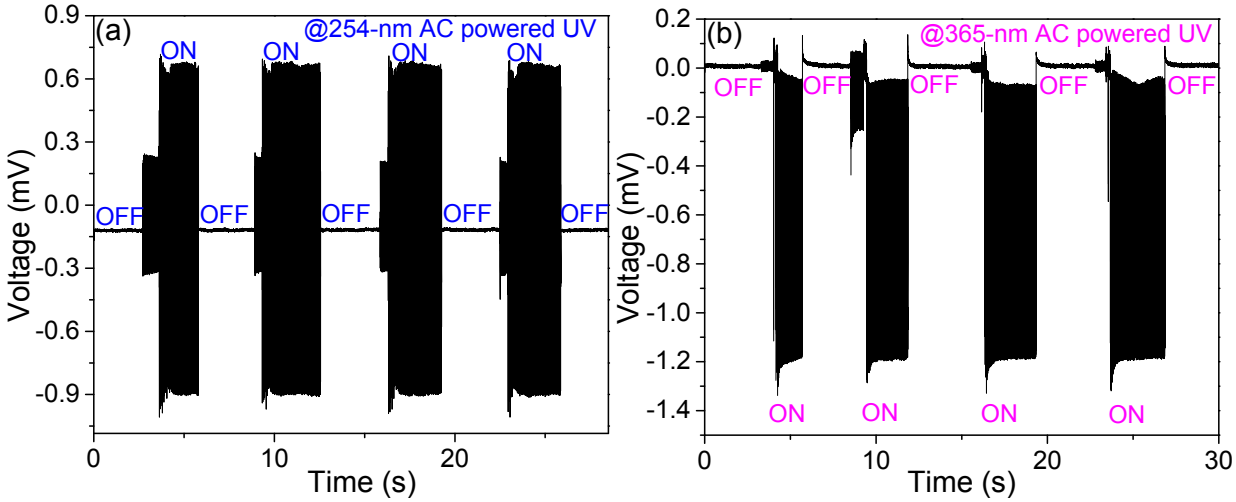

Fig. S12 On-off photovoltages of LiCl:$FAPbCl_3$-based photodetector under 254-nm (a) and 365-nm (b) AC-powered UV illuminations.

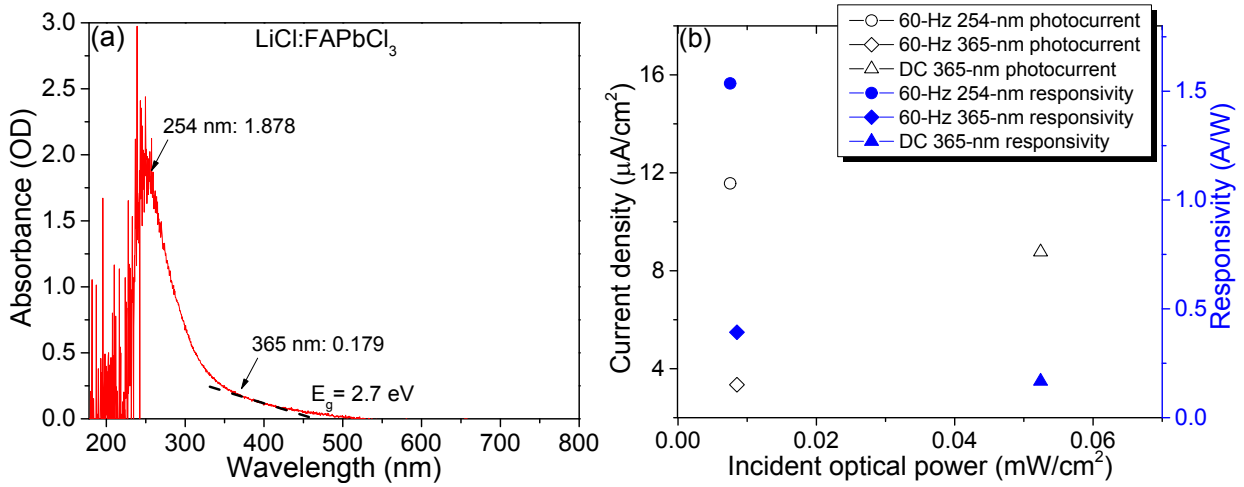

Fig. S13 UV-Vis absorbance spectrum of $LiCl:FAPbCl_3$ nanostructured film, which shows an absorption onset at around 460 nm (a), and summary of photocurrent densities (left y-axis) with corresponding responsivities (right y-axis) of $LiCl:FAPbCl_3$ (b).

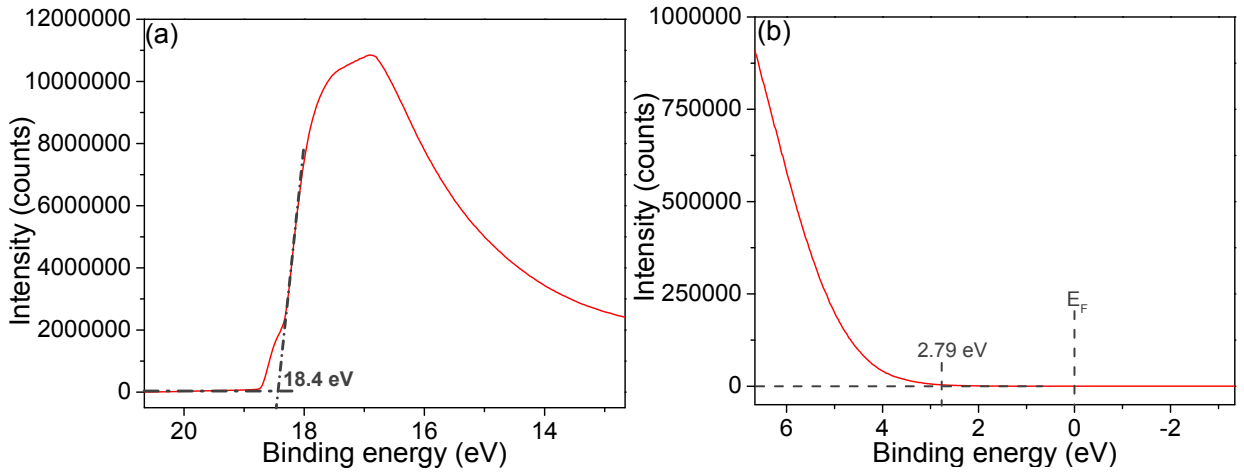

Fig. S14 Ultraviolet photoelectron spectra (UPS) of LiCl:$FAPbCl_3$ nanostructured film. UPS in the ranges of 12 - 20 eV (a), -3 - 6 eV (b) of electron binding energies. Based on the shown spectrum intersections with baseline (18.4 eV and 2.79 eV), the width of binding energy is determined as ΔE = 18.4 eV - (2.79 eV) = 15.6 eV, which leads to the valence band maximum of LiCl:$FAPbCl_3$ as: 15.6 eV - 21.2 eV (He I UV photon) = -5.6 eV.[20-23]

REFERENCES

1. Zhu, H.; Fu, Y.; Meng, F.; Wu, X.; Gong, Z.; Ding, Q.; Gustafsson, M. V.; Trinh, M. T.; Jin, S.; Zhu, X-Y. *Nat. Mater.* **2015**, *14*, 636-642.

2. Fu, Y.; Zhu, H.; Stoumpos, C. C.; Ding, Q.; Wang, J.; Kanatzidis, M. G.; Zhu, X.; Jin, S. *ACS Nano* **2016**, *10*, 7963-7972.

3. Govinda, S.; Kore, B. P.; Swain, D.; Hossain, A.; De, C.; Row, T. N. G.; Sarma, D. D. *J. Phys. Chem. C* **2018**, *122*, 13758-13766.

4. Maculan, G.; Sheikh, A. D.; Abdelhady, A. L.; Saidaminov, M. I.; Haque, M. A.; Murali, B.; Alarousu, E.; Mohammed, O. F.; Wu, T.; Bakr, O. M. *J. Phys. Chem. Lett.* **2015**, *6*, 3781-3786.

5. Jun, J. H.; Seong, H.; Cho, K.; Moon, B.-M.; Kim, S. *Ceram. Int.* **2009**, *35*, 2797-2801.

6. Zhang, J.; Wang, Q.; Zhang, X.; Jiang, J.; Gao, Z.; Jin, Z.; Liu, S. (F.) *RSC Adv.* **2017**, *7*, 36722-36727.

7. Jin, Y.; Wang, J.; Sun, B.; Blakesley, J. C.; Greenham, N. C. *Nano Lett.* **2008**, *8*, 1649-1653.

8. Tian, W.; Zhai, T.; Zhang, C.; Li, S.-L.; Wang, X.; Liu, F.; Liu, D.; Cai, X.; Tsukagoshi, K.; Golberg, D.; Bando, Y. *Adv. Mater.* **2013**, *25*, 4625-4630.

9. Gundimeda, A.; Krishna, S.; Aggarwal, N.; Sharma, A.; Sharma, N. D.; Maurya, K. K.; Husale, S.; Gupta, G. *Appl. Phys. Lett.* **2017**, *110*, 103507.

10. Ahmed, A. A.; Devarajan, M.; Afzal, N. *Sens. Actuator A-Phys.* **2017**, *262*, 78-86.

11. Xue, H.; Kong, X.; Liu, Z.; Liu, C.; Zhou, J.; Chen, W. *Appl. Phys. Lett.* **2007**, *90*, 201118.

12. Xing, J.; Zhao, K.; Lu, H. B.; Wang, X.; Liu, G. Z.; Jin, K. J.; He, M.; Wang, C. C.; Yang, G. Z. *Opt. Lett.* **2007**, *32*, 2526-2528.

13. Xing, J.; Guo, E.; Jin, K.-j.; Lu, H.; Wen, J.; Yang, G. *Opt. Lett.* **2009**, *34*, 1675-1677.

14. Guo, E.-J.; Xing, J.; Jin, K.-J.; Lu, H.-B.; Wen, J.; Yang, G.-Z. *J. Appl. Phys.* **2009**, *106*, 023114.

15. Guo, E.-J.; Xing, J.; Lu, H.-B.; Jin, K.-J.; Wen, J.; Yang, G.-Z. *J. Phys. D* **2009**, *43*, 1.

16. Bera, A.; Peng, H.; Lourembam, J.; Shen, Y.; Sun, X. W.; Wu, T. *Adv. Funct. Mater.* **2013**, *23*, 4977-4984.

17. Jin, K. X.; Zhai, Y. X.; Li, H.; Tian, Y. F.; Luo, B. C.; Wu, T. *Solid State Commun.* **2014**, *199*, 39-42.

18. Zhang, Z.; Zheng, W.; Lin, R.; Huang, F. *R. Soc. open sci.* **2018**, *5*, 180905.

19. Wang, W.; Xu, H.; Cai, J.; Zhu, J.; Ni, C.; Hong, F.; Fang, Z.; Xu, F.; Cui, S.; Xu, R.; Wang, L.; Xu, F.; Huang, J. *Opt. Express* **2016**, *24*, 8411-8419.

20. Jiang, Q.; Zhang, L.; Wang, H.; Yang, X.; Meng, J.; Liu, H.; Yin, Z.; Wu, J.; Zhang, X.; You, J. *Nat. Energy* **2016**, *2*, 16177.

21. Endres, J.; Egger, D. A.; Kulbak, M.; Kerner, R. A.; Zhao, L.; Silver, S. H.; Hodes, G.; Rand, B. P.; Cahen, D.; Kronik, L.; Kahn, A. *J. Phys. Chem. Lett.* **2016**, *7*, 2722-2729.

22. Wang, C.; Liu, X.; Wang, C.; Xiao, Z.; Bi, C.; Shao, Y.; Huang, J.; Gao, Y. *J. Vac. Sci. Technol.* **2015**, *33*, 032401.

23. Wang, S.; Sakurai, T.; Wen, W.; Qi, Y. *Adv. Mater. Interfaces* **2018**, 5, 1800260.